DISTRIBUTION OF REDUCED SEISMIC ENERGY AND STRESS DROP IN THE ALTAI-SAYAN SEISMOACTIVE REGION

N.A. Sycheva [1✉], L.M. Bogomolov [2]

[1] Schmidt Institute of Physics of the Earth, Russian Academy of Sciences, 10-1 Bolshaya Gruzinskaya St, Moscow 123242, Russia

[2] Institute of Marine Geology and Geophysics, Far Eastern Branch of the Russian Academy of Sciences, 1B Nauki St, Yuzhno-Sakhalinsk 693022, Russia

ABSTRACT. The data bank has been created to address the tensor of the seismic moment of earthquakes that occurred in the Altai-Sayan seismically active region in the period 1978–2025. The scalar seismic moment M_0 for these events was already known from the CMT catalog. This paper presents estimates of the following dynamic parameters: source radius r, shear stress drop $\Delta\sigma$, and reduced seismic energy e_{PR} using a phenomenological approach based on previously obtained regression relationships between the source radius r and the scalar seismic moment M_0. Stress drop and reduced seismic energy estimates have been obtained for 69 earthquakes with a magnitude M_W 3.5–7.2. Thus, it allows to significantly expand the data bank on these earthquake parameters for the Altai-Sayan seismically active region. Maps have been drawn of the areally averaged estimates of stress drop and reduced seismic energy.

1. INTRODUCTION

The development of new approaches to predicting destructive earthquakes and mitigating the destruction of earthquakes may, if necessary, involve increasing the amount of data on the dynamic parameters: source radius r, scalar seismic moment M_0 and shear stress drop (hereinafter for short stress drop, $\Delta\sigma$), acting parallel to the fault plane. The information on these parameters, directly related to the earthquake source volume, and on the reduced seismic energy (the seismic energy to moment ratio: $e_{PR}=E_S/M_0$) may characterize regional features of the geodeformational process. The crustal stress field is one of the main factors taken into account when assessing the predicted earthquake magnitude. Tectonic features such as faults, folds, fractures and volcanos, are the results of the impact of stresses. Stress drop in the earthquake sources is a key parameter that determines how much energy is released in an earthquake. Besides, the temporal variation of the averaged stress drops for the events of given magnitudes reflects the state of stress in the Earth's crust on the Coulomb-Mohr diagram. Such description of the Earth's crust in the seismoactive regions requires a statistically significant dataset – a sufficiently large number of seismic events for which the dynamic source parameters have been determined. Also of interest is the comparison between the distributions of kinematic (focal) source parameters and dynamic parameters of seismotectonic deformations (STD). Note that kinematic and dynamic parameters of earthquake sources can both be referred to as source parameters, though "source parameters" in some publications imply only dynamic parameters [Sycheva, Bogomolov, 2016].

As known, determining dynamic parameters of earthquakes requires plotting source spectrum of their seismograms, which identifies spectral density Ω_0 (contribution of the lowest-frequency harmonics) and angular frequency f_0 (the parameter describing a decrease in the amplitudes of high-frequency harmonics). The obtained Ω_0 values may serve as a basis for the scalar seismic moment calculation using the known formula [Riznichenko, 1985] which describes $M_0\sim\Omega_0$ proportionality, with the coefficient of proportionality determined only by the parameters of the medium in the source zone. The data obtained on the angular frequency allow estimating the source radius ($r\sim1/f_0$) to an accuracy of the coefficient depending on the source motion model (since there are models of seismic wave radiation) [Riznichenko, 1985; Scholz, 2002]. The best known are the Brune, Madariaga and some other models (a review is provided in [Sycheva, Bogomolov, 2020]). For such calculations of scalar seismic moment and source radius it is important that M_0 does not depend on angular frequency f_0, and that Ω_0 does not influence radius r.

The stress drops may be calculated by the formula [Kostrov, 1975; Scholz, 2002]:

$$\Delta\sigma = 7M_0 / 16r^3, \qquad (1)$$

showing that the $\Delta\sigma$ value is proportional to $\Omega_0 f_0^3\sim M_0 f_0^3$. Because of this, the errors of angular frequency and source radius estimation lead to the substantially larger $\Delta\sigma$ error.

According to the source fault model [Madariaga, 2011], the value of the reduced seismic energy can be calculated using the formula:

$$e_{PR} = 2M_0 f_0^3 / (GV_S^3), \qquad (2)$$

where G is the shear modulus of the rocks in the source zone, and V_s is the transverse wave velocity ($G=\rho V_S^2$, ρ is a density). Since $r\sim1/f_0$, the stress drop and reduced seismic energy values are proportional to each other [Kocharyan, 2016]. The transition from $\Delta\sigma$ to e_{PR} may involve the translation formula [Sycheva, Bogomolov, 2020]:

$$e_{PR} = (32k^3 / 7)\Delta\sigma / G, \qquad (3)$$

where k is a numerical coefficient depending on the source model and equal to k=0.37 for the Brune model [Brune, 1970, 1971] and to k =0.26 for the improved Madariaga – Kaneko – Shearer model [Kaneko, Shearer, 2014]. It is important to emphasize that the reduced seismic energy, unlike the stress drops, does not depend on the source model selection, as it follows from (2). In addition, the $k^3\Delta\sigma$ in (3) is the same for the Brune, Madariaga – Kaneko – Shearer and other models, since $\Delta\sigma\sim1/r^3\sim1/k^3$ [Sycheva, Bogomolov, 2020].

In [Kocharyan, 2014, 2016] it is substantiated that the seismic sources are self-similar when e_{PR} values are statistically independent on seismic moment M_0 and not self-similar when there is the regression (approximate relationship) between e_{PR} and M_0. In this connection, of interest is a multiple determination of stress drops and/or reduced seismic energy. The results of such research obtained for the North Tien Shan are presented in the discussion section of [Sycheva et al., 2020]. Using this region as an example, a procedure has been developed for calculating dynamic parameters of the sources of 2.60–5.35 magnitude earthquakes and M=6 Kochkor earthquake of December 25, 2006. An integral part of this work is the transition from the station spectrum of seismograms to the source spectrum, which requires determining medium quality factor. Consequently, the task of calculation of the stress drops requires high-quality seismic records and considerable computational resources for determining spectral parameters Ω_0 and f_0. The error of the angular frequency estimation is therewith often larger than Ω_0, because of what the publications usually provide the data only on seismic moment M_0.

When considering the earthquakes for which the scalar seismic moment is known (the data source is described below), it implies that the estimation of stress drops and reduced seismic energy may involve regression dependency of source radius on energy characteristic (M_0, or moment magnitude M_W). This implies the use of model dependencies (regressions) which were proposed in publications, generalizing the data on dynamic parameters in the study region or other regions, or theoretically substantiated. The present paper involves such approach for estimating $\Delta\sigma$ and e_{PR} of the earthquakes in the Altai-Sayan mountain region.

The aim is to create (expand) the data bank of all dynamic parameters based on the data for 69 earthquakes,

whose seismic moments are known and which occurred in the study region during 1978–2025 time period. To choose a suitable method for approximating relationship between the source radius and moment magnitude, consideration has been given to different regressions obtained in [Rizni-chenko, 1985; Dobrynina, 2009; Zavyalov, Zotov, 2021; Kim et al., 1989; Boore, 2003; Bormann et al., 2009; Sycheva, Bogomolov, 2020]. Considering the specific features of these regressions, differing in M_W range, the averaged model has been constructed for the dependency of source radius on energy characteristic of the event.

Altai-Sayan upland is an area of an active orogenic process still continuing today, as evidenced by numerous strong modern earthquakes. The analysis of the present-day kinematics of the lithospheric blocks in Central Asia [Sankov et al., 2002; Abdrakhmatov et al., 1996; Larson et al., 1999] shows that the Indian – Eurasia collision deter-mines only those intracontinental deformations which are localized west of the 105th meridian.

Fig. 1 shows the epicentral location of earthquakes from the catalog of the GS RAS (Geophysical Survey RAS; http://www.gsras.ru/) for the Altai-Sayan region from 1997 to 2021. The stations of the Altai-Sayan Branch GS RAS allow recording earthquakes not only in the Altai-Sayan mountain region but also in the adjacent areas – East Kazakhstan, Mongolian Altai, Northern Mongolia, and South Pribaikalye. The same map shows the epicenters of strong $M \geq 6$ earth-

quakes occurred there since 1761 (see the caption to Fig. 1). Fig. 1 displays the block boundaries after [Sankov et al., 2003]. Most of strong earthquakes occurred at the block boundary [Emanov et al., 2023]. Many of these earthquakes took place near the Tuva-Mongolian block boundaries [Emanov et al., 2023]. Notable in the seismicity structure is a seismically activated block structure covering the Tuva-Mongolian block together with the eastern part of the Tuva upland [Emanov et al., 2023].

The most unique aftershock process took place after the 1991 Busingol earthquake. There occurred a pulse mode with short-term (~1-month) activation, recurring during more than twenty years. The mode change occurred in 2010, but seismic activity of this epicentral zone is still continuing. The 2011–2012 Tuva earthquakes [Emanov et al., 2014a] took place in the Kaa-Khem fault zone, in aseis-mic area during instrumental period [Emanov et al., 2023]. The source zone of two similar-energy earthquakes was formed as a single, still high-activity structure. North of the 1991 Busingol earthquake, seismic activity intensified in the mountains bordering the Belin rift basin [Emanov et al., 2010, 2014b, 2021]. Seismic studies of the Prikhubsugulye revealed the change in the stress state therein relative to the Baikal-type basins [Misharina et al., 1983], as well as that the Khubsugul basin seismicity does not correspond to the structure or tectonic position of the basin [Logachev, 1993], which anticipated seismic activation in 2021 [Emanov et
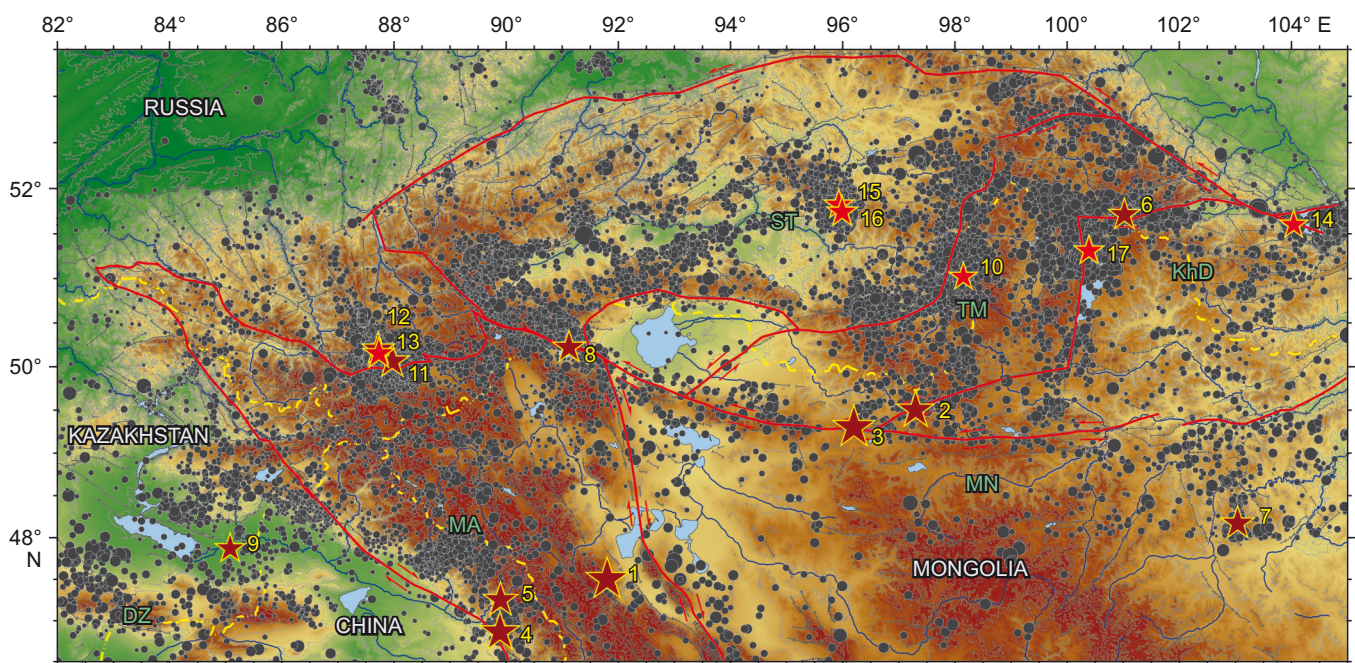

Fig. 1. Epicentral location of earthquakes in the Altai-Sayan mountain region (from the catalogue of the GS RAS, over 22000 events, 1997–2021).

Stars mark strong earthquakes: red – $M \geq 6$ earthquakes; dark red – with $M \geq 7$ earthquakes. Earthquake numbers are shown in yellow: 1 – Great Mongolian, 1761, M=8.3; 2 – Tannu-Ola, 1905, M=7.6; 3 – Bolnai, 1905, M=8.3; 4 – Fuyun, 1931, M=7.9; 5 – aftershock of the Fuyun earthquake, 1931, M=7.3; 6 – Mondy, 1950, M=7.0; 7 – Mogod, 1967, M=7.0; 8 – Ureg-Nur, 1970, M=7.0; 9 – Zaysan, 1990, M=6.8; 10 – Busingol, 1991, M=6.4; 11 – Chuya, 2003, M=7.3; 12 – aftershock of the Chuya earthquake, 2003, M=7.0; 13 – aftershock of the Chuya earthquake, 2003, M=6.9; 14 – Kultuk, 2008, M=6.4; 15 – Tuva I, 2011, M=6.6; 16 – Tuva II, 2012, M=6.8; 17 – Khubsugul, 2021, M=6.9. Letters indicate blocks [Sankov et al., 2003]: ST – Sayan-Tuva, TM – Tuva-Mongolian, KhD – Khamar Daban, MA – Mongolian Altai, DZ – Dzungar, MN – Mongolian.

al., 2022]. After 2021, high activity is observed along the entire block structure borders. Principally new is the occurrence of the Darkhat earthquake swarm where seismicity has not previously been observed. No earthquakes have occurred there since 1963. They took place after the 2021 Khubsugul earthquake. Seismically active axial line of the Darkhat basin and activation did not previously affect the area of earthquake swarm generation. The earthquake swam occurred in the eastward protrusion of the basin in the central part at the bending mountain range that separates the Darkhat and Khubsugul basins.

2. INITIAL DATA AND METHODOLOGY

As a source material, consideration is being given to the earthquakes in the Altai-Sayan mountain region and adjacent areas, for which the scalar seismic moment has been calculated. The earthquake data are listed in the Centroid Moment Tensor (CMT) catalog (https://www.global cmt.org/CMTsearch.html). Alongside the components of the seismic moment tensor, this data source includes scalar seismic moment M_0 and moment magnitude M_W. These parameters were obtained for 66 earthquakes occurred in the Altai-Sayan mountain region from 1978 to 2025. Fig. 2 shows the seismic moment tensors of these earthquakes. To 66 events from the CMT catalog (Fig. 2), we added 3 earthquakes of 2003 (the Chuya earthquake aftershocks) from the GS RAS catalog with reported moment magnitude and scalar seismic moment, thus having increased the considered earthquake number to 69. In Fig. 2, the epicentral location of these earthquakes is highlighted in blue. The

seismic moment tensors (CMT catalog) and epicenters of three earthquakes (GS RAS catalog) are shown on the background distribution of annual earthquake numbers, calculated based on the data presented in Fig. 1 (GS RAS catalog earthquakes from 1997 to 2001). The quantitative distribution of earthquakes was calculated in 1×1° cells (the data volume greater than 22 000 events allows considering a ~100×100 km area), with only representative part of the catalog (2≤M≤7.3 earthquakes) taken into account [Sycheva, Sychev, 2022]). Dark-green color stands for the cells with an annual earthquake number N>15. The maximum annual earthquake number (73 events) is marked in the cell centered at 50.5° N and 87.5° E (source area of the 2003 Chuya earthquake); setting upper limit for legend (N=73) would have led to a reflection of only one zone – the Chuya earthquake area. A significant part of the considered earthquakes (69 events) falls within the cells with high seismicity level.

Fig. 3 presents some quantitative characteristics of 69 earthquakes: the moment magnitude of earthquakes varying from 4 to 7.2, a large number of earthquakes (68 %) with magnitude of M_W=4.75–5.5 (Fig. 3, a), most of the earthquakes occurred after 2000 (Fig. 3, b), and the maximum number of earthquakes reached in 2003 (Chuya earthquakes and its aftershocks). The earthquakes occurred at depths ranging from 10 to 35 km; the depths of three GS RAS catalogue earthquakes have not yet been determined. The depth of these events is assigned to be 15 km (Fig. 3, c), as in [Kuchai, 2012], which analyzes the focal mechanisms of earthquakes in the Altai and Sayan and notes that the
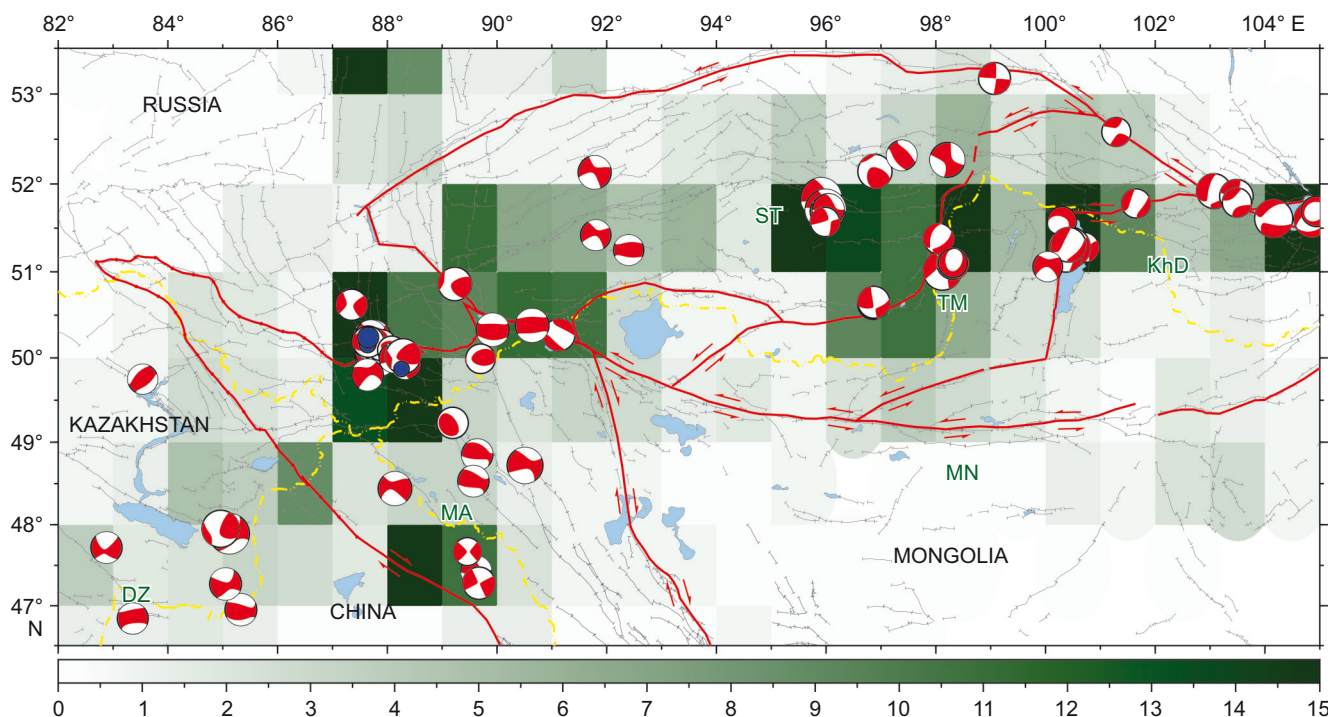
Fig. 2. Seismic moment tensors (CMT) for the earthquakes in the Altai, Sayan and adjacent areas (66 events) against the background of the annual earthquake number (more than 22000 events from 1997 to 2021 in the GS RAS catalog).
Gray lines are faults after [Bachmanov et al., 2017]. The dash-dotted line is the state border. Blue color stands for the epicenters of the earthquakes (3 events) from the GS RAS catalog for which the scalar seismic moment is known. See Fig. 1 for the block names.

depth was set equal to 15 km because of the lack of the accurate determination of the earthquake focal depths in the Altai-Sayan mountain region.

To select a model that relates the source radius to magnitude M_W, we consider the examples of regressions from the publications on the study of dynamic parameters, referred to above in the introduction section. Relationships $r(M_W)$ obtained therein are summarized in Table 1, which also presents the characteristic features of each model.

[Borman et al., 2009] present the amplitude spectra A of moderate ground motion regarding frequency f, scaled at seismic moment M_0 and equivalent moment value M_W. It is noted that the maximum seismic energy E_S is radiated at the angular frequency f_c, which is presented in the paper for each moment magnitude value ranging from 4.5 to 9 with a 0.5 step size. These data served as a basis for calculating the source radius for the Brune model [Brune, 1970, 1971], performing distribution of the radius of moment magnitude, and deriving the regression equation for the events with $M_W \geq 4.5$.

In [Boore, 2003], theoretical consideration is given to a simple but powerful method for modeling ground motions, which is to combine parametric or functional descriptions of the ground-motion amplitude spectrum with a random phase spectrum, modified such that the motion is distributed over the duration related to the earthquake magnitude and to the distance from the source. This simple method has been successful in matching different ground motion parameters for earthquakes with seismic moments spanning more than 12 orders of magnitude (which corresponds to the earthquakes with $M_W > 2.5$) in diverse tectonic environments.

The discussion section in [Riznichenko, 1985, p. 32], relating the source radius to the magnitude and class of an earthquake, presents the results from [Chinnery, 1961, 1969; and other papers], dealing with analysis of strong earthquakes. In [Zavyalov, Zotov, 2021], which considers the most common characteristics of the relationship between a typical dimension of the earthquake source and its magnitude, a regression dependence was obtained, nearly coincident with the result from [Riznichenko, 1985] in the magnitude range from 5.5 to 8.5.

In [Sycheva, Bogomolov, 2020; Dobrynina, 2009; Kim et al., 1989], consideration is being given to the dynamic parameters of earthquakes occurred in different regions: North Tien Shan, Baikal rift zone, and Baltic Shield, respectively. In [Vakov, 1988], it is shown that the relationships between magnitude and source dimensions for normal crustal earthquakes beyond the boundaries of the Benioff zone are mainly determined by the type of motion and do not depend much on the regional conditions, which allows considering the publications on dynamic parameters of earthquakes in terms of regions. These publications analyze the events, most of which are weak (magnitude range

Table 1. Model relationships between the source radius (m) and the moment magnitude; the number and range of magnitudes of the studied events; the source

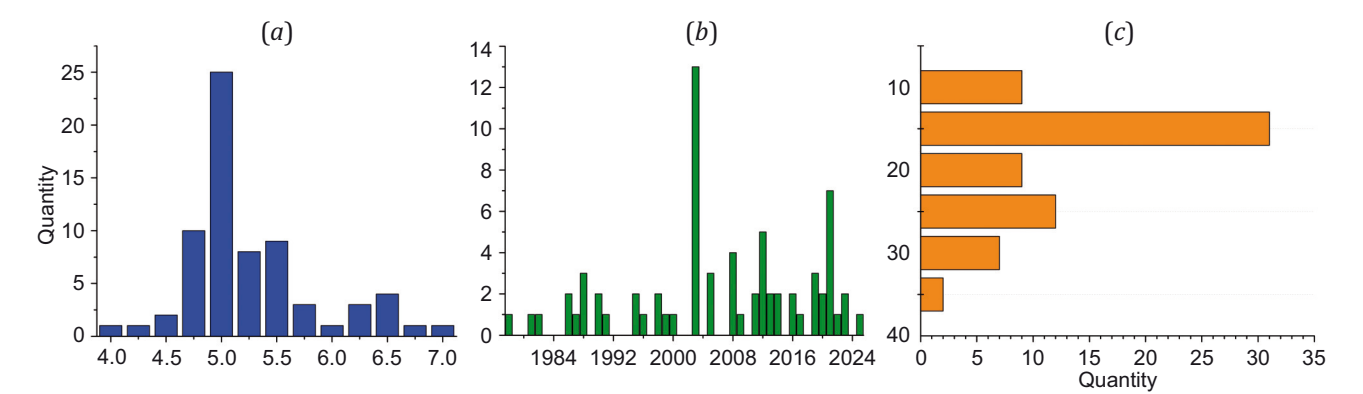| No.	lg(r, [m])	Number of events	Magnitude range M_W	Source
		Theoretical		
1	$0.5M_W+0.85$	Not applicable	4.5–9.0	[Bormann et al., 2009]
2	$0.5M_W+0.58$	–/–	3.0–8.0	[Boore, 2003]
3	$0.4M_W+1.50$	–/–	0.12–9.20	[Riznichenko, 1985]
		Experimental		
4	$0.2M_W+1.80$	183	2.5–5.5	[Sycheva, Bogomolov, 2020]
5	$0.1M_W+2.60$	63	1.7–6.1	[Dobrynina, 2009]
6	$0.22M_W+2.02$	90	1.6–4.2	[Kim et al., 1989]

Fig. 3. Quantitative distribution of the earthquakes under consideration (69 events): (*a*) – by magnitude, (*b*) – by year, (*c*) – by depth.

for each region is shown in Table 1). Only single events had a moment magnitude greater than 5. However, theoretical studies have proposed the relationships between wide-range magnitudes and source dimensions for earthquakes including the strongest events listed in Table 1. That is why it is rather nontrivial to select a model or a way of combining models. Fig. 4, a, shows the relationships between the source radius logarithm and moment magnitude in accordance with the sources referred to in Table 1. Each of the model regressions is shown within a magnitude range for which it has been determined. It is worthy of note that there is a similarity between the plots for model [Borman et al., 2009] and models [Riznichenko, 1985; Zavyalov, Zotov, 2021] within the magnitude range $4.5 < M_W < 8$. Such relationship is rather nontrivial because in [Borman et al., 2009] the source (Brune) radius is determined from the displacement spectrum parameters and characterizes seismic wave radiation, and the approach in [Zavialov, Zotov, 2021] is based on the analysis of the hypocenter distribution of the aftershocks and assesses the dimensions of the fault that emerged after the main shock. This may indicate a wide applicability of the model in the discussion section of [Riznichenko, 1985].

However, the angular coefficient in the considered theoretical models differs significantly from that in the models based on experiments. This may be due to a lack of statistics on large earthquakes in models 4–6 in Table 1. Fig. 4, b, along with regressions in Table 1, shows logarithmic mean radius $(\lg r)_{AV}$ depending on M_W in different magnitude intervals (gray line) and a linear regression plot $(\lg r)_{AV}$ (crimson-colored line). Averaging has been carried out with regard to the number of models applicable to the considered magnitude values in the range $M_W = 3.5–7.2$, which is of interest in terms of further application in the analysis of dynamic parameters of earthquakes in the Altai-Sayan mountain region. The averaged relationship between $(\lg r)_{AV}$ and magnitude M_W appeared broken-line due to the changes in the number of models in the points where regression of any type either starts or stops.

The averaged values $\lg r$ were used to derive the linear regression equation

$$\lg(r_B[m]) = 0.45 M_W + 0.96, \quad (4)$$

where index "B" implies that the consideration is being given to the source radius in the Brune model [Brune, 1970, 1971]. The coefficient of determination R^2, determining the relationship between model (4) and averaged relationship $(\lg r)_{AV}$ (a gray line in Fig. 4, b), is 0.67. According to [Aivazyan, Mkhitaryan, 2001], such model is acceptable since $R^2 > 0.5$. Pearson correlation coefficient between the relationships shown in Fig 4, b, by the gray and crimson-colored lines is $\rho = 0.84$. In case of a linear regression, $\rho = (R^2)^{1/2}$ [Aivazian, Mkhitarian, 2001; Aivazian, 2001].

The obtained model regression is most similar to the model in [Borman et al., 2009].

To derive a convenient equation which allows calculating stress drops based on the known values of magnitude M_W or seismic moment M_0, we calculate the logarithm of (1) and substitute linear regression (4) into the obtained expression instead of $\lg r$. As a result, we obtain:

$$\lg(\Delta\sigma[MPa]) = \lg(7/16) + \lg(M_0[N \cdot m]) - 1.35 M_W - 8.88. \quad (5)$$

If to express a moment magnitude in (5) in terms of seismic moment using the Kanamori formula [Kanamori, 1977]

$$M_W = 2/3(\lg(M_0[N \cdot m]) - 9.1), \quad (6)$$

it would be easy to derive the final expression:

$$\lg(\Delta\sigma[MPa]) = 0.1 \cdot \lg(M_0[N \cdot m]) - 1.05. \quad (7)$$

The expression, which relates the stress drops to the moment magnitudes and is equivalent to (7), can be equated to:

$$\lg(\Delta\sigma[MPa]) = 0.15 M_W - 0.14. \quad (8)$$

For the reduced seismic energy whose values are proportional to $\Delta\sigma$, the regression dependencies analogous to (7) and (8) are also true. After substituting the values
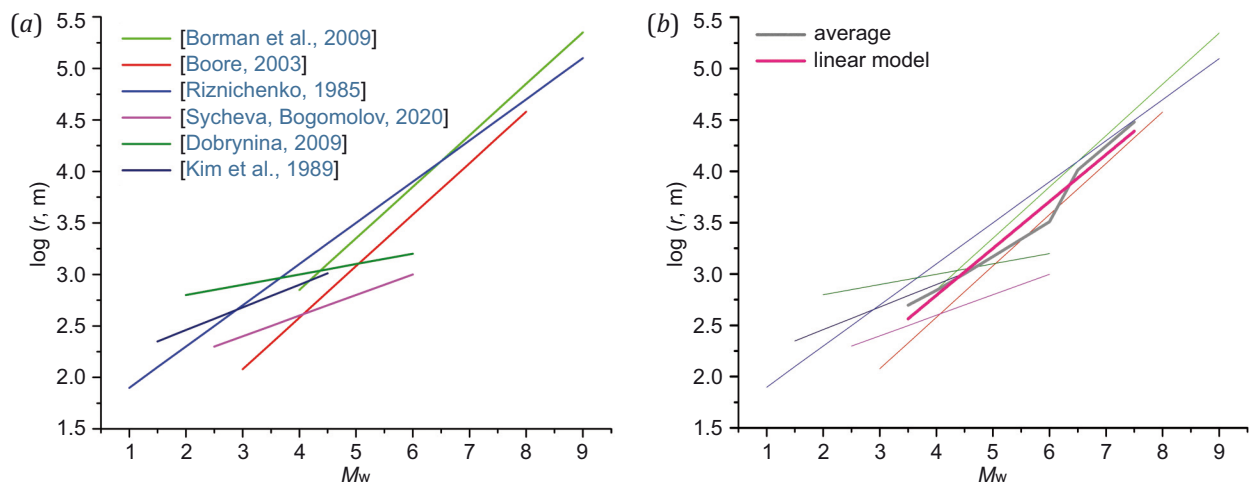

Fig. 4. Dependence of the source radius r_B on the moment magnitude M_W for the models under consideration (a) (Table 1), and the average value for the models and its regression (b).

of shear modulus $G\cong2\cdot10^3$ MPa and coefficient k for the Brune model–k=0.37 – in (3), calculating the logarithm of (3) and changing lg $(\Delta\sigma)$ according to (7) and (8), the following expressions can be obtained:

$$\lg e_{PR}=0.1\cdot\lg(M_0[N\cdot m])-4.97, \lg e_{PR}=0.15M_W-4.06. \quad (9)$$

3. RESULTS

The approach described in the methodology section was used to calculate the source radius, stress drops and reduced seismic energy for 65 earthquakes considered. App. 1, Table 1.1 presents the results of calculation of r and $\Delta\sigma$ for the Brune model. Also shown are relative values of the radiuses and stress drops; the M_W=7.2 Chuya earthquake of September 27, 2003 was selected as a reference. The source radius of this earthquake in the Brune model r=~15800 m, the stress drop value $\Delta\sigma$=~10 MPa.

App. 1, Table 1.1 also contains the reduced seismic energy value, which, as mentioned above, does not depend on the source model selection. The typical order of magnitude of e_{PR} of the M=4–5 earthquakes is ~10^{-3}, with corresponds to the results in [Dobrynina, 2009; Kocharyan, 2012]. For the earthquakes considered (M_W=3.7–7.2), the average source radius is 2932 m, medium source radius – 1995 m, the average stress drop corresponds to 4.72 MPa, the medium stress drop – to 4.23 MPa, the average value of e_{PR}=0.57·10^{-3}, the medium e_{PR}=0.51·10^{-3}. Some difference between the average (mean) and medium values of the considered parameters is caused by the fact that 80 % of earthquakes vary in magnitude in the range 4.2–5.7, which is responsible for some deviations in the calculated parameters.

Fig. 5 presents the epicentral location of 69 earthquakes studied, with a circle fill color depending on the stress drop value (see the map legend that shows range $\Delta\sigma$ for each of the selected colors and the corresponding number of earthquakes) on the background distribution of the logarithm of seismotectonic deformation intensity [Lukk, Yunga, 1979], obtained in [Sycheva, 2023] for the Altai-Sayan mountain region. Most of the considered events fell within the areas where seismotectonic deformation intensity exceeds 10^{-10} year^{-1} (source areas of the 2003 Chuya earthquake, 2021 Khubsugul earthquake, 2011–2012 Tuva earthquakes).

The verification of stress drop and reduced seismic energy estimates, made using regressions (7) – (9), i.e. by the phenomenological method, may involve the results presented in [Zakharova et al., 2009; Chepkunas, Malyanova, 2017, 2018], where the source spectra served as a basis for determining dynamic parameters of some strong earthquakes worldwide, including 5 earthquakes in the Altai-Sayan region. The data on dynamic parameters, obtained by both methods, are available for the following earthquakes (Fig. 6):

– Chuya earthquake, September 27, 2003, M_W=7.2 (No. 20 in App. 1, Table 1.1);

– aftershock of the Chuya earthquake, September 27, 2003, M_W=6.4 (No. 21);

– aftershock, October 1, 2003, M_W=6.6 (No. 22);

– I Tuva earthquake, December 29, 2011, M_W=6.7 (No. 41);

– II Tuva earthquake, February 26, 2012, M_W=6.6 (No. 42).

For these 5 earthquakes, Table 2 presents the values of some dynamic parameters determined by two methods. In the papers whose authors are the members of the staff of the Geophysical Survey RAS and referred to herein, the
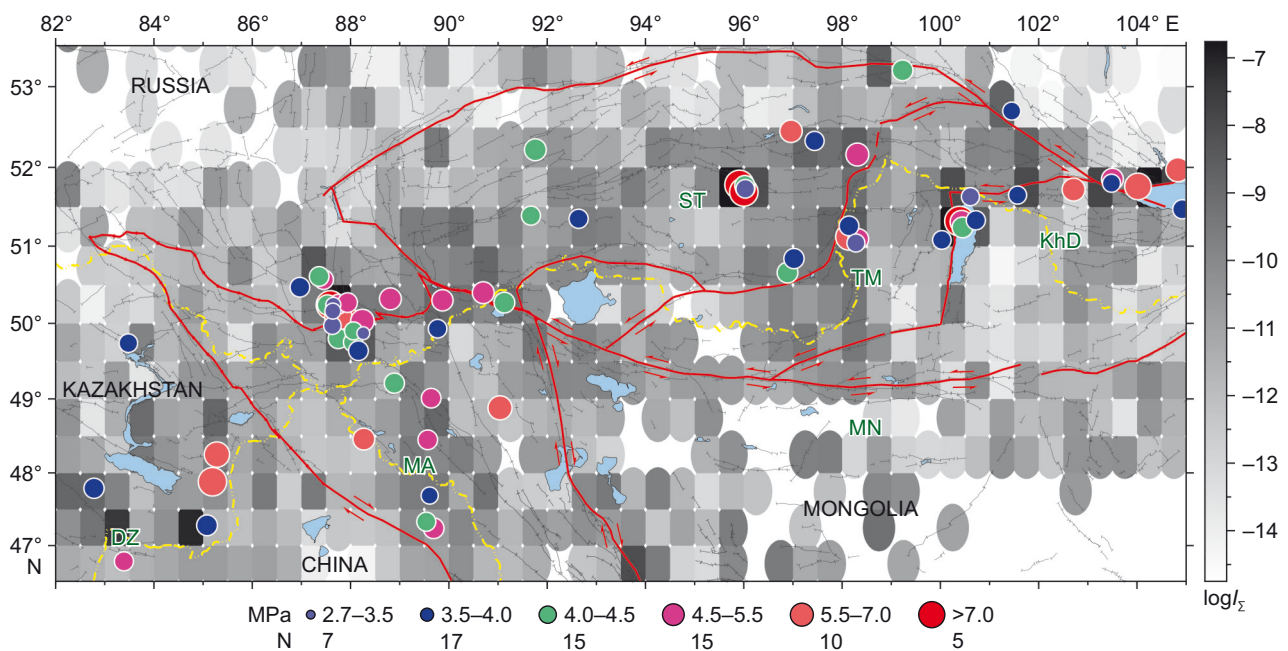

Fig. 5. Epicentral location of the earthquakes studied.
The color of the circle fill depends on the magnitude of the released stresses (see the map legend). The released stresses are calculated using the Brune earthquake source model [Brune, 1970, 1971]. For block names, see Fig. 1.
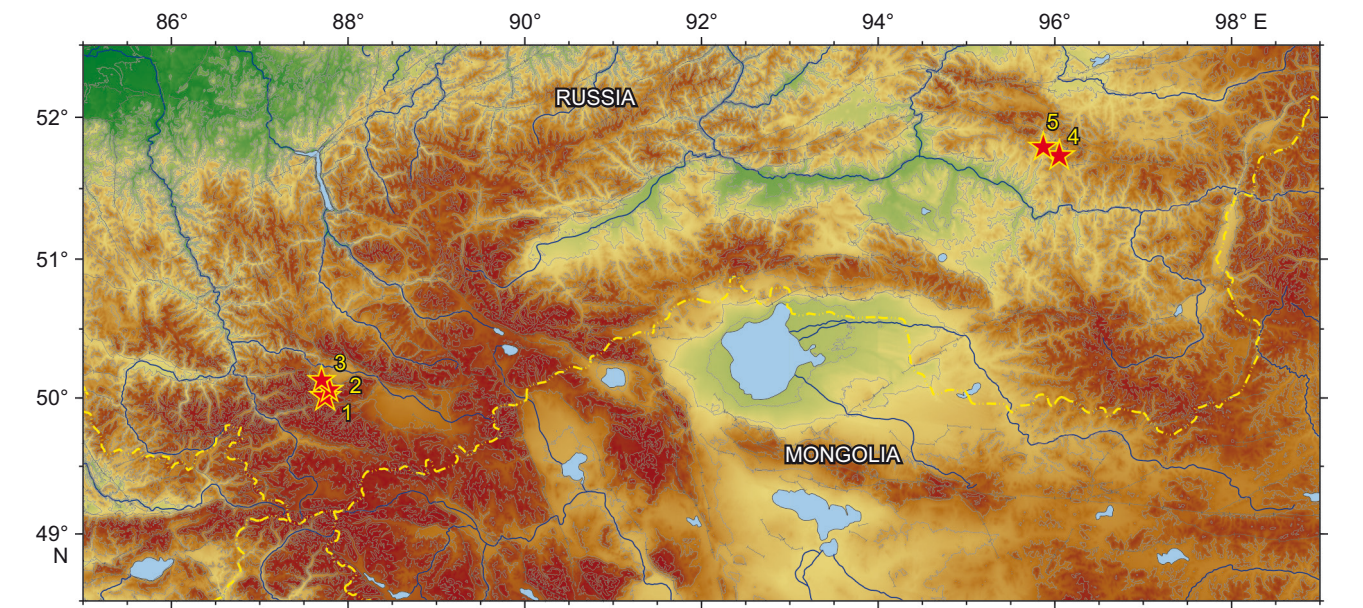
Fig. 6. Epicentral location of test earthquakes (5 events). The earthquake number corresponds to the number in Table 2.

Table 2. The values of scalar seismic moment, rupture length L, source radius and shear stress drop, according to [Zakharova et al., 2009; Chepkunas, Malyanova, 2017, 2018] and the results presented here (App. 1, Table 1.1)

No.	Date	Time	From the source spectrum				Phenomenological approach			
			M_W	$M_0 \cdot 10^{19}$, N·m	$L \cdot 10^3$, m	$\Delta\sigma \cdot 10^5$, N/m^2	M_W	$M_0 \cdot 10^{19}$, N·m	$r_B \cdot 10^3$, m	$\Delta\sigma \cdot 10^5$, N/m^2
1	September 27, 2003	11:33:26.5	6.9	2.2	24	56	7.2	9.38	15.8	103.1
2	September 27, 2003	18:52:47.1	6.2	0.2	9	96	6.4	0.45	6.92	60
3	October 1, 2003	01:03:25.0	6.3	0.4	9	**192**	6.6	1.13	8.51	**80**
4	December 27, 2011	15:21:54.9	6.6	0.9	14	115	6.7	1.38	9.44	72
5	February 26, 2012	06:17:18.0	6.8	1.5	18	90	6.6	1.2	8.5	84
			Average of $\Delta\sigma \cdot 10^5$			110	Average of $\Delta\sigma \cdot 10^5$			80
			Weighted average of $\Delta\sigma \cdot 10^5$			76.5	Weighted average of $\Delta\sigma \cdot 10^5$			92.6

dynamic parameters are calculated based on the spectra of longitudinal waves obtained with STS-1 seismometers at teleseismic distances Δ≤100° from the data recorded by "Obninsk" station (OBN; 55.1146° N, 36.5674° E; h=160 m). The epicentral distance interval for the considered earthquakes varies in the range Δ=30.9–34.7°. According to [Zakharova et al., 2009; Chepkunas, Malyanova, 2017, 2018], the station spectra of the earthquakes mentioned (Table 2) were reduced to the source before determining spectral parameters Ω_0 and f_0.

In the analysis of Table 2, attention is drawn to the discrepancy between the scalar seismic moment value and source dimension obtained by two different methods. For M_0, on the one hand, it is due to the fact that the scalar seismic moment in [Zakharova et al., 2009; Chepkunas, Malyanova, 2017, 2018] was determined by spectral parameters of longitudinal, not of transverse waves. On the other hand, the discrepancies in M_0 (i.e. in energy characteristics) may be caused by the hypocentral depth error in the CMT catalog for the earthquakes considered. In pub-

lications which involved spectral parameters, the largest source dimension (source length) was determined by the Haskell's, not by the Brune model (the model review in [Aptekman et al., 1989]), so that the difference between L and r values in Table 2 is not surprising. Dynamic parameters M_0, r, L are intermediate in stress drop estimations. In view of the foregoing, when comparing values $\Delta\sigma$, obtained by two methods, the question arises about a compatibility or incompatibility at least in the order of values.

According to Table 2, the calculation based on the source spectrum gave higher stress drops than that based on regressions in 4 out of 5 cases. The ratio $\Delta\sigma_{spectrum}/\Delta\sigma_{regression}$ does not exceed 1.6 in 3 cases and reaches 2.4 in 1 case (aftershock of the 27.09.2003 Chuya earthquake). For the Chuya earthquake, there is an inverse ratio between the values $\Delta\sigma$: $\Delta\sigma_{spectrum} \sim 0.55 \Delta\sigma_{regression}$. The magnitudes of 5 earthquakes considered lie in a narrow range, and the arithmetic mean $\Delta\sigma$ becomes important there. For two methods of stress drop calculation, the average values presented in Table 2 differ by approximately 20 %. There is the

same difference in the weighted average of the values $\Delta\sigma$ for two methods. For the calculations from the spectra, the arithmetic mean turned out to be larger and the weighted average turned out to be smaller than for the regression-based method.

Thus, the difference in the stress drop values for two methods is less than one order of magnitude (maximum 2.4 times), which implies the possibility to use the obtained data (App. 1, Table 1.1) for $\Delta\sigma$ and for e_{PR}, proportional thereto, in the Altai-Sayan region. However, for the aftershocks of the Chuya earthquake, whose magnitudes are lower and stress drops are higher than those of the main shock, the parameters are not consistent with regression. This shows that in case of aftershocks the proposed phenomenological approach may lead to errors.

4. DISCUSSION

The stress drop values are related to the source area, i.e. to a rather small volume of the medium. The analysis of the relationship among the stress drops, geodynamic environments and the large-scale averaged parameters of the stress-strain state of the earth's crust requires averaging $\Delta\sigma$ over some event sampling. The sampling in the study region was performed by 1×1° zoning. The volumes of sources, in which the shear stress drops occur, are different for different events and represent different proportions of the volume of the medium for the study zone. Therefore, the averaging of the stress drops over sampling naturally involves introducing weighting coefficient g_i, proportional to the source volume, i.e. $g_i \sim r_i^3$, where i is an event number in the sampling. The weighted average of the stress drops $<\Delta\sigma>_{AW}$ will be determined by the expression:

$$< \Delta\sigma >_{AW} = \sum_i g_i \Delta\sigma_i / \sum_i g_i = \sum_i \Delta\sigma_i r_i^3 / \sum_i r_i^3. \quad (10)$$

Since $\Delta\sigma_i r_i^3 = 7/16(M_0)_i$, this expression can be reduced to the following calculation formula for the weighted average of the stress drops:

$$< \Delta\sigma >_{AW} = \frac{7}{16} \sum_i (M_0)_i / \sum_i r_i^3, \quad (11)$$

where the summation is performed over all sample events, M_{0i}, is a scalar seismic moment of the earthquake number "i", and r_i is the source radius value calculated by the Brune model.

Averaging resulted in obtaining $\Delta\sigma_{AW}$ for 36 cells of size 1×1°. 24 cells were contacted by 1 event, and the averaged $\Delta\sigma_{AW}$ corresponds to the stress drop during an earthquake. For the rest of the cells, the averaged $\Delta\sigma_{AW}$ depends on the number of earthquakes in a cell.

Fig. 7, a, shows the ellipse-shaped cells for which the values $\Delta\sigma_{AW}$ have been obtained. To visualize (to map) the calculation results, use has been made of the GMT program nearneighbor (Generic Mapping Tools, https://www.generic-mapping-tools.org/), which implements the nearest neighbor algorithm to assign the average value to every node which has one or several points within the assigned radius therefrom. This program considers a node as the center of an elliptical (circular) zone to which the calculated average applies. A cell color depends on value

of the logarithmic average of the stress drops (logarithmic scale provides more contrasting delineation patterns of the cells with the minimum stress drop value). Each cell shows the number of events fell therein. Most of the events fell within the cell which coincides with the source area of the Chuya earthquake. The dark-blue cells (15 of 36) have $\Delta\sigma_{AW} \leq 4$ MPa, and 7 zones have $\Delta\sigma_{AW} \geq 6.5$ MPa (source area of the Chuya earthquake ~9 MPa, Tuva earthquakes ~8 MPa, Busingol earthquake ~6.5 MPa etc.).

High stress drop falls within the northern boundaries of the Mongolian-Altai block (the Chuya earthquake area, Septmber 27, 2003, M_W=7.2, and further east), northwestern and southeastern boundaries of the Tuva-Mongolian block, southeastern part of the Sayan-Tuva block; high stress drop is also typical of Jungar block area (Fig. 7, a).

Fig. 7, b, presents the logarithmic distribution of the total reduced seismic energy, calculated also for 1×1° cells. The proper value lge_{PR} is shown for the cells contacted only by one event. It is natural that the areal distribution of lg(Σe_{PR}) is similar to the distribution of lg$\Delta\sigma_{AW}$ (Fig. 7, a) due to (4). Some differences (the cells south of the northern boundaries of the Mongolian-Altai block) are caused by the fact that the summation of e_{PR} within a cell is performed irrespectively of the source volumes. Fig. 7, b, depicts zones with the maximum values of total e_{PR}: the northern boundary of the Mongolian-Altai block, $\Sigma e_{PR} \sim (0.8-6.0) \cdot 10^{-3}$, and the northwestern and southeastern boundaries of the Tuva-Mongolian block, $\Sigma e_{PR} \sim (0.2-3.0) \cdot 10^{-3}$.

As a result of the application of the phenomenological approach for calculating the source radius (without plotting the source spectrum of earthquake seismograms), an assessment was made of the shear stress drops and reduced seismic energy for 69 earthquakes occurred in the Altai-Sayan mountain region. This allowed the comparison between $\Delta\sigma$ and e_{PR} for different events and different zones (App. 1, Table 1.1 presents for convenience the relative values $\Delta\sigma$).

To compare the stress drop value (dynamic parameter) with the Lode – Nadai coefficient distribution (kinematic parameter), the joint mapping of these parameters was carried out for the study area (Fig. 8). The considered parameters were compared within the area for which the Lode – Nadai coefficient distribution has been obtained [Sycheva, Rebetsky, 2024]. From among the events considered, 59 fell within the cells with the known values of the Lode – Nadai coefficient. The calculation was made of the number of events and of the total stress drop for the earthquakes in the areas with different deformation modes which were determined by the Lode – Nadai coefficient value. Table 3 presents some results of the quantitative analysis. In the areas of uniaxial extension ($\mu_\varepsilon \leq -0.6$, blues in the legend), there are no events considered.

According to the data presented in Table 2, 26 (~44 %) earthquakes are located in the area of uniaxial compression deformation and uniaxial compression dominance. The total stress drop, an average with weighting factor proportional to the source volume $\Delta\sigma_{AW}$, calculated by (11), was 4 MPa. The pure shear deformation area is associated
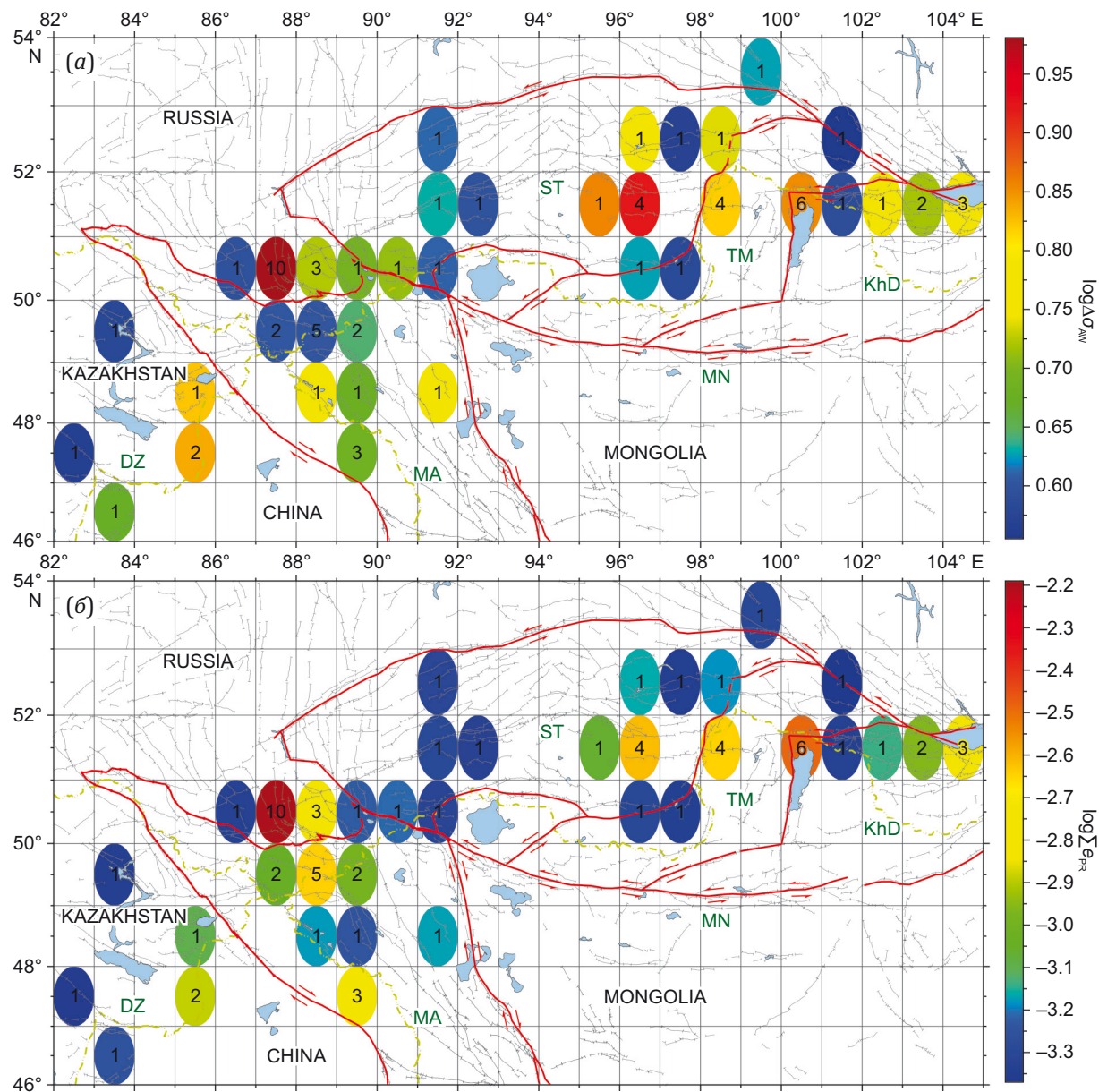
Fig. 7. Distribution of logarithm values: (*a*) – dropped stresses Δσ$_{AW}$; (*b*) – total reduced seismic energy. The numbers indicate the number of events fell therein. For block names, see Fig. 1.

Table 3. The stress drop values Δσ and the Lode – Nadai coefficient μ_ε [Sycheva, Rebetsky, 2024] in zones of different defotmation modes

Factor	Deformation modes				
	Uniaxial compression	Uniaxial compression dominance	Pure shear	Uniaxial compression	Uniaxial extension
μ_ε	$0.6 \le \mu_\varepsilon \le 1.0$	$0.2 < \mu_\varepsilon < 0.6$	$-0.2 \le \mu_\varepsilon \le 0.2$	$-0.6 < \mu_\varepsilon < -0.2$	$-1.0 \le \mu_\varepsilon \le -0.6$
Δσ$_{AW}$, MPa	4.0	8.9	7.3	5.6	0
N	2	24	27	6	0

with localization of 27 (~46 %) earthquakes and the stress drop Δσ$_{AW}$ of 8.9 MPa. In the area of the uniaxial extension dominance, there are 6 (10 %) earthquakes, and the stress drop Δσ$_{AW}$ was 5.6 MPa. When the kinematic characteristics of earthquakes are compared to their dynamic characteristics, it is apparent that most of the stress drops occurred in the areas with $\mu_\varepsilon > 0.2$, which corresponds to the mode of uniaxial compression deformation and uniaxial compression dominance. The source area of the Chuya earthquake is associated with the mode of uniaxial compression dominance (Fig. 8). The stress drop during the Chuya earthquake was ~10 MPa.

Fig. 8. Epicentral location of earthquakes on the background distribution of the Lode – Nadai coefficient, after [Sycheva, Rebetsky, 2024].
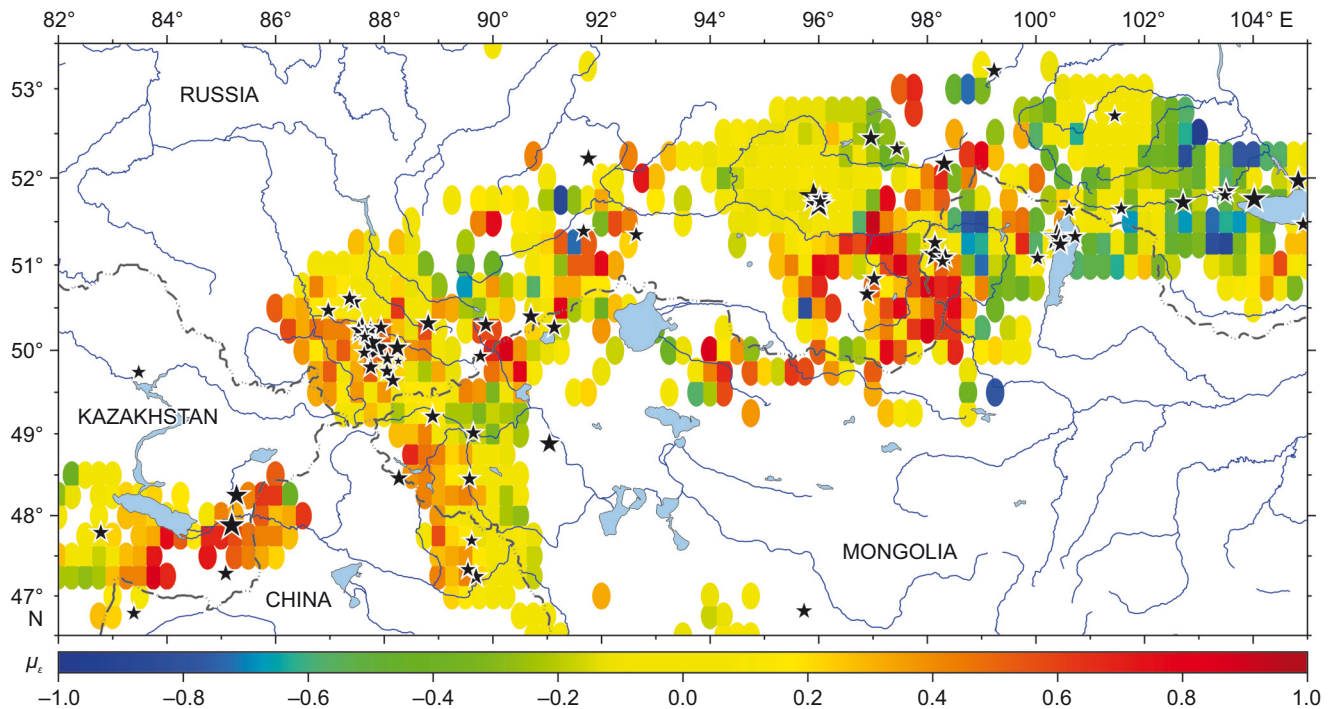
Concluding the description of the distributions of reduced seismic energy and stress drops for the earthquakes in the Altai-Sayan region, we emphasize the features of the proposed phenomenological method. This method is based on the generalizations concerning the relationship between the source radius and scalar seismic moment (or moment magnitude). The phenomenological model (regression) considers a large amount of data from different publications. This does not require determination of the values of angular frequencies, which are often scattered. Nevertheless, the applicability of the phenomenological method for other seismoactive regions remains a question, which should be considered in each individual case (it is particularly important to recognize how small the proportion of aftershocks is in the sample with a known seismic moment). The proposed method for assessing stress drops and reduced seismic energy will make it possible to increase significantly the available data concerning dynamic parameters.

5. CONCLUSION

The present paper proposes the phenomenological approach to the calculation of the source radius without plotting a source spectrum. Analysis has been made on the previously determined theoretical and empirical relationships between the source radius and the moment magnitude. Averaging of these relationships served as a basis for derivation of the expressions for calculating the shear stress drops and reduced seismic energy from the data on the scalar seismic moment or the moment magnitude. The proposed approach has been used for the earthquakes in the Altai-Sayan mountain region to increase the amount of data on the stress drops $\Delta\sigma$ and reduced seismic energy e_{PR}.

There is a correspondence between the regression-based estimates of stress drops for 5 test earthquakes (phenomenological approach) and the estimates previously calculated from the source spectral parameters.

Among the earthquakes that hit this area in 1978–2025, there were selected 69 events whose scalar seismic moments and moment magnitudes (M_W=4.75–5.50) are listed in the CMT catalog. Regarding these events, the estimates have been made on $\Delta\sigma$ and e_{PR}, and the databank has been compiled from the dynamic parameters (App. 1, Table 1.1). For mapping the areal stress drop distributions, it has been proposed to use the weighted averages $\Delta\sigma$, considering the difference in source volumes of the averaged (compactly located) events. For most of the 1×1° zones, in which the stress drop averaging was performed, the values $\Delta\sigma_{AW}$ do not exceed 4.5 MPa, and the maximum weighted average stress drop $\Delta\sigma_{AW}$ is ~9 MPa. The same zones in the study area are characterized by the reduced seismic energy values e_{PR}~0.58·10⁻³.

A comparative analysis of the kinematic and dynamic parameters of earthquakes has shown that most of the stress drops $\Delta\sigma_{AW}$ fell within the areas with μ_ε>0.2, which corresponds to the mode of uniaxial compression deformation and uniaxial compression dominance.

6. CONTRIBUTION OF THE AUTHORS

Both authors made an equivalent contribution to this article, read and approved the final manuscript.

7. DISCLOSURE

The authors declare that they have no conflicts of interest relevant to this manuscript.

8. REFERENCES

Abdrakhmatov K.Ye., Aldazhanov S.A., Hager B.H., Hamburger M.W., Herring T.A., Kalabaev K.B., Makarov V.I., Molnar P. et al., 1996. Relatively Recent Construction of the Tien Shan Inferred from GPS Measurements of Present-Day Crustal Deformation Rates. Nature 384, 450–453. https://doi.org/10.1038/384450a0.

Aivazian S.A., 2001. Applied Statistics. Essentials of Econometrics. Vol. 2. Essentials of Econometrics. Textbook. Unity-Dana, Moscow, 432 p. (in Russian) [Айвазян С.А. Прикладная статистика. Основы эконометрики. Т. 2. Основы эконометрики: Учебник. М.: Юнити-Дана, 2001. 432 с.].

Aivazian S.A., Mkhitarian V.S., 2001. Applied Statistics. Essentials of Econometrics. Vol. 1. Theory and Applied Statistics. Textbook. Unity-Dana, Moscow, 656 p. (in Russian) [Айвазян С.А., Мхитарян В.С. Прикладная статистика. Основы эконометрики. Т. 1. Теория вероятностей и прикладная статистика: Учебник. М.: Юнити-Дана, 2001. 656 с.].

Aptekman Zh.Ya., Belavina Yu.F., Zakharova A.I., Zobin V.M., Kogan S.Ya., Korchagina O.A., Moskvina A.G., Polikarpova L.A., Chepkunas L.S., 1989. P-wave Spectra in the Context of Determining the Dynamic Source Parameters of Earthquakes. Station to Source Spectrum Transition and Calculation of Dynamic Source Parameters. Journal of Volcanology and Seismology 2, 66–79 (in Russian) [Аптекман Ж.Я., Белавина Ю.Ф., Захарова А.И., Зобин В.М., Коган С.Я., Корчагина О.А., Москвина А.Г., Поликарпова Л.А., Чепкунас Л.С. Спектры Р-волн в задаче определения динамических параметров очагов землетрясений. Переход от станционного спектра к очаговому и расчет динамических параметров очага // Вулканология и сейсмология. 1989. № 2. С. 66–79].

Bachmanov D.M., Kozhurin A.I., Trifonov V.G., 2017. The Active Faults of Eurasia Database. Geodynamics & Tectonophysics 8 (4), 711–736 (in Russian) [Бачманов Д.М., Кожурин А.И., Трифонов В.Г. База данных активных разломов Евразии // Геодинамика и тектонофизика. 2017. Т. 8. № 4. С. 711–736]. https://doi.org/10.5800/GT-2017-8-4-0314.

Boore D., 2003. Simulation of Ground Motion Using the Stochastic Method. Pure and Applied Geophysics 160 (3–4), 635–676. https://doi.org/10.1007/PL00012553.

Bormann P., Liu R., Xu Z., Ren K., Zhang L., Wendt S., 2009. First Application of the New IASPEI Teleseismic Magnitude Standards to Data of the China National Seismographic Network. Bulletin of the Seismological Society of America 99 (3), 1868–1891. https://doi.org/10.1785/0120080010.

Brune J.N., 1970. Tectonic Stress and the Spectra of Seismic Shear Waves from Earthquakes. Journal of Geophysical Research 75 (26), 4997–5009. https://doi.org/10.1029/JB075i026p04997.

Brune J.N., 1971. Correction [to "Tectonic Stress and the Spectra of Seismic Shear Waves from Earthquakes"]. Journal of Geophysical Research 76 (20), 5002. https://doi.org/10.1029/JB076i020p05002.

Chepkunas L.S., Malyanova L.S., 2017. Source Parameters of Strong Earthquakes. Earthquakes of the Northern Eurasia. Iss. 20 (2011). GS RAS, Obninsk, p. 277–281 (in Russian) [Чепкунас Л.С., Малянова Л.С. Очаговые параметры сильных землетрясений Земли // Землетрясения Северной Евразии. Обнинск: ФИЦ ЕГС РАН, 2017. Вып. 20 (2011 г.). С. 277–281].

Chepkunas L.S., Malyanova L.S., 2018. Source Parameters of Strong Earthquakes. Earthquakes of the Northern Eurasia. Iss. 21 (2012). GS RAS, Obninsk, p. 280–285 (in Russian) [Чепкунас Л.С., Малянова Л.С. Очаговые параметры сильных землетрясений Земли // Землетрясения Северной Евразии. Обнинск: ФИЦ ЕГС РАН, 2018. Вып. 21 (2012 г.). С. 280–285].

Chinnery V.A., 1961. The Deformation of the Ground Around Surface Faults. Bulletin of the Seismological Society of America 51 (3), 355–3725. https://doi.org/10.1785/BSSA0510030355.

Chinnery V.A., 1969. Earthquake Magnitude and Source Parameters. Bulletin of the Seismological Society of America 59 (5), 1969–1982. https://doi.org/10.1785/BSSA0590051969.

Dobrynina A.A., 2009. Source Parameters of the Earthquakes of the Baikal Rift System. Izvestiya, Physics of the Solid Earth 45 (12), 1093–1109. https://doi.org/10.1134/S1069351309120064.

Emanov A.F., Emanov A.A., Chechel'nitskii V.V., Shevkunova E.V., Radziminovich Ya.B., Fateev A.V., Kobeleva E.A., Gladyshev E.A., Arapov V.V., Artemova A.I., Podkorytova V.G., 2022. The Khuvsgul Earthquake of January 12, 2021 (M_W=6.7, M_L=6.9) and Early Aftershocks. Izvestiya, Physics of the Solid Earth 58, 59–73. https://doi.org/10.1134/S1069351322010025.

Emanov A.F., Emanov A.A., Chechelnitsky V.V., Shevkunova E.V., Kobeleva E.A., Fateev A.V., 2023. The Block Structure and the Strongest Earthquakes of the Junction Area Between the Altai-Sayan Mountain Region and the Baikal Rift Zone. In: Problems of Complex Geophysical Monitoring of Seismoactive Regions. Proceedings of the 9th Scientific-Technical Conference with an International Participation (September 24–30, 2023). Kamchatka Branch of the GS RAS, Petropavlovsk-Kamchatsky, p. 139–142 (in Russian) [Еманов А.Ф., Еманов А.А., Чечельницкий В.В., Шевкунова Е.В., Кобелева Е.А., Фатеев А.В. Блоковая структура и сильнейшие землетрясения стыка Алтае-Саянской области и Байкальской рифтовой зоны // Проблемы комплексного геофизического мониторинга сейсмоактивных регионов: Труды Девятой всероссийской научно-технической конференции с международным участием (24–30 сентября 2023 г.). Петропавловск-Камчатский: КФ ФИЦ ЕГС РАН, 2023. С. 139–142].

Emanov A.F., Emanov A.A., Fateev A.V., Soloviev V.M., Shevkunova E.V., Gladyshev E.A., Antonov I.A., Korabelshchikov D.G. et al., 2021. Seismological Studies in the Altai-Sayan Mountain Region. Russian Journal of Seismology 3 (2), 20–51 (in Russian) [Еманов А.Ф., Еманов А.А., Фатеев А.В., Соловьев В.М., Шевкунова Е.В., Гладышев Е.А., Антонов И.А., Корабельщиков Д.Г. и др. Сейсмологические

исследования на территории Алтае-Саянской горной области // Российский сейсмологический журнал. 2021. Т. 3. № 2. С. 20–51]. https://doi.org/10.35540/2686-7907.2021.2.02.

Emanov A.F., Emanov A.A., Leskova E.V., 2010. Seismic Activation in the Busingol-Belinsky Fault Zone. Physical Mesomechanics 13 (S1), 72–77 (in Russian) [Еманов А.Ф., Еманов А.А., Лескова Е.В. Сейсмические активизации в Белино-Бусингольской зоне // Физическая мезомеханика. 2010. Т. 13. № S1. С. 72–77].

Emanov A.F., Emanov A.A., Leskova E.V., Seleznev V.S., Fateev A.V., 2014a. The Tuva Earthquakes of December 27, 2011, M_L=6.7, and February 26, 2012, M_L=6.8, and Their Aftershocks. Doklady Earth Sciences 456 (1), 594–597. https://doi.org/10.1134/S1028334X14050249.

Emanov A.F., Leskova E.V., Emanov A.A., Radziminovich Ya.B., Gileva N.A., Artemova A.I., 2014b. The August 16, 2008, Belin-Bii-Khem Earthquake with K_P=15, M_W=5.7, I_0=7 (the Tuva Republic). Earthquakes of the Northern Eurasia. Iss. 17 (2008). GS RAS, Obninsk, p. 378–385 (in Russian) [Еманов А.Ф., Лескова Е.В., Еманов А.А., Радзиминович Я.Б., Гилёва Н.А., Артёмова А.И. Белин-Бий-Хемское землетрясение 16 августа 2008 г. с K_P=15, M_W=5.7, I_0=7 (Республика Тыва) // Землетрясения Северной Евразии. Обнинск: ГС РАН, 2014. Вып. 17 (2008 г.). С. 378–385].

Kanamori H., 1977. The Energy Release in Great Earthquakes. Journal of Geophysical Research 82 (20), 2981–2987. https://doi.org/10.1029/JB082i020p02981.

Kaneko Y., Shearer P.M., 2014. Seismic Source Spectra and Estimated Stress Drop Derived from Cohesive-Zone Models of Circular Subshear Rupture. Geophysical Journal International 197 (2), 1002–1015. https://doi.org/10.1093/gji/ggu030.

Kim W.-Y., Wahlström R., Uski M., 1989. Regional Spectral Scaling Relations of Source Parameters for Earthquakes in the Baltic Shield. Tectonophysics 166 (1–3), 151–161. https://doi.org/10.1016/0040-1951(89)90210-2.

Kocharyan G.G., 2012. On Radiation Efficiency of Earthquakes (an Example of Geomechanical Interpretation of the Results of Seismological Observations). Dynamic Processes in Geospheres 3, 36–47 (in Russian) [Кочарян Г.Г. Об излучательной эффективности землетрясений (пример геомеханической интерпретации результатов сейсмологических наблюдений) // Динамические процессы в геосферах. 2012. № 3. С. 36–47].

Kocharyan G.G., 2014. Scale Effect in Seismotectonics. Geodynamics & Tectonophysics 5 (2), 353–385 (in Russian) [Кочарян Г.Г. Масштабный эффект в сейсмотектонике // Геодинамика и тектонофизика. 2014. Т. 5. № 2. С. 353–385]. https://doi.org/10.5800/GT-2014-5-2-0133.

Kocharyan G.G., 2016. Geomechanics of Faults. GEOS, Moscow, 424 p. (in Russian) [Кочарян Г.Г. Геомеханика разломов. М.: ГЕОС, 2016. 424 с.].

Kostrov B.V., 1975. Mechanics of Tectonic Earthquake Source. Nauka, Moscow, 176 p. (in Russian) [Костров Б.В. Механика очага тектонического землетрясения. М.: Наука, 1975. 176 с.].

Kuchai O.A., 2012. Specific Features of Fields of Stresses Associated with Aftershock Processes in the Altai-Sayan Mountainous Region. Geodynamics & Tectonophysics 3 (1), 59–68 (in Russian) [Кучай О.А. Особенности поля напряжений афтершоковых процессов землетрясений Алтае-Саянской горной области // Геодинамика и тектонофизика. 2012. Т. 3. № 1. С. 59–68]. https://doi.org/10.5800/GT-2012-3-1-0062.

Larson K.M., Bürgmann R., Bilham R., Freymueller J.T., 1999. Kinematics of the India-Eurasia Collision Zone from GPS Measurements. Journal of Geophysical Research: Solid Earth 104 (B1), 1077–1093. https://doi.org/10.1029/1998JB900043.

Logachev N.A. (Ed.), 1993. Seismotectonics and Seismicity of Lake Khövsgöl Region. Nauka, Novosibirsk, 184 p. (in Russian) [Сейсмотектоника и сейсмичность Прихубсугулья / Ред. Н.А. Логачев. Новосибирск: Наука, 1993. 184 с.].

Lukk A.A., Yunga S.L., 1979. Seismotectonic Deformation of the Garm Region. Bulletin of the USSR Academy of Sciences. Physics of the Earth 10, 24–43 (in Russian) [Лукк А.А., Юнга С.Л. Сейсмотектоническая деформация Гармского района // Известия АН СССР. Физика Земли. 1979. № 10. С. 24–43].

Madariaga R., 2011. Earthquake Scaling Laws. In: R. Meyers (Ed.), Extreme Environmental Events: Complexity in Forecasting and Early Warning. Springer, New York, p. 364–383. https://doi.org/10.1007/978-1-4419-7695-6_22.

Misharina L.A., Melnikova V.I., Baljinnyam I., 1983. South-Western Boundary of the Baikal Rift Zone from the Data on Earthquake Focal Mechanisms. Volcanology and Seismology 2, 74–83 (in Russian) [Мишарина Л.А., Мельникова В.И., Балжинням И. Юго-западная граница Байкальской рифтовой зоны по данным о механизме очагов землетрясений // Вулканология и сейсмология. 1983. № 2. С. 74–83].

Riznichenko Yu.V., 1985. Problems of Seismology. Nauka, Moscow, 408 p. (in Russian) [Ризниченко Ю.В. Проблемы сейсмологии. М.: Наука, 1985. 408 с.].

Sankov V.A., Levi K.G., Lukhnev A.V., Miroshnichenko A.I., Parfeevets A.V., Radziminovich N.A., Melnikova V.I., Deverchere J. et al., 2002. Recent Geodynamics of the Mongol-Siberian Mobile Belt from the Geological-Structural and Instrumental Data. In: Tectonics and Geophysics of the Lithosphere. Proceedings of the XXXV Tectonic Meeting (January 1 – December 31, 2002). Vol. 2. GEOS, Moscow, p. 170–174 (in Russian) [Саньков В.А., Леви К.Г., Лухнев А.В., Мирошниченко А.И., Парфеевец А.В., Радзиминович Н.А., Мельникова В.И., Девершер Ж. и др. Современная геодинамика Монголо-Сибирского подвижного пояса по данным геолого-структурных и инструментальных исследований // Тектоника и геофизика литосферы: Материалы XXXV Тектонического совещания (1 января – 31 декабря 2002 г.). М.: ГЕОС, 2002. Т. 2. С. 170–174].

Sankov V.A., Lukhnev A.V., Miroshnichenko A.I., Levi K.G., Ashurkov S.V., Bashkuev Yu.B., Dembelov M.G., Calais E. et al., 2003. Present-Day Movements of the Earth's Crust in the

Mongol-Siberian Region Inferred from GPS Geodetic Data. Doklady Earth Sciences 393 (8), 1082–1085.

Scholz C.H., 2002. The Mechanics of Earthquakes and Faulting. Cambridge University Press, Cambridge, 496 p. https://doi.org/10.1017/CBO9780511818516.

Sycheva N.A., 2023. Study of Seismotectonic Deformations of the Earth's Crust in the Altai-Sayan Mountain Region. Part I. Geosystems of Transition Zones 7 (3), 223–242 (in Russian) [Сычева Н.А. Исследование сейсмотектонических деформаций земной коры Алтае-Саянской горной области. Часть I // Геосистемы переходных зон. 2023. Т. 7. № 3. С. 223–242]. https://doi.org/10.30730/gtrz.2023.7.3.223-242.

Sycheva N.A., Bogomolov L.M., 2016. Patterns of Stress Drop in Earthquakes of the Northern Tien Shan. Russian Geology and Geophysics 57 (11), 1635–1645. https://doi.org/10.1016/j.rgg.2016.10.009.

Sycheva N.A., Bogomolov L.M., 2020. On the Stress Drop in North Eurasia Earthquakes Source Versus Specific Seismic Energy. Geosystems of Transition Zones 4 (4), 393–446. https://doi.org/10.30730/gtrz.2020.4.4.393-416.417-446.

Sycheva N.A., Bogomolov L.M., Kuzikov S.I., 2020. Computational Technologies in Seismological Research (on the Example of KNET, Northern Tien Shan). IMGG FEB RAS, Yuzhno-Sakhalinsk, 358 p. (in Russian) [Сычева Н.А., Богомолов Л.М., Кузиков С.И. Вычислительные технологии в сейсмологических исследованиях (на примере KNET, Северный Тянь-Шань). Южно-Сахалинск: ИМГиГ ДВО РАН, 2020. 358 с.]. https://doi.org/10.30730/978-5-6040621-6-6.2020-2.

Sycheva N.A., Rebetsky Yu.L., 2024. Comparing the STD- and MCA-Based Estimates of the Crustal Deformation in the Altai-Sayan Mountain Region. In: Tectonophysics and Challenges in Earth Sciences. Proceedings of the Sixth Tectonophysical Conference to the 300th Anniversary of the Russian Academy of Sciences (October 7–12, 2024). IPE RAS, Moscow, p. 329–336 (in Russian) [Сычева Н.А., Ребецкий Ю.Л. Сравнение некоторых оценок деформации земной коры Алтае-Саянской горной области, полученных на основе методов СТД и МКА // Тектонофизика и актуальные вопросы наук о Земле: Материалы Шестой тектонофизической конференции, приуроченной к 300-летию Российской академии наук (7–12 октября, 2024 г.). М.: ИФЗ РАН, 2024. С. 329–336].

Sycheva N.A., Sychev V.N., 2022. Some Characteristics of Seismicity in the Altai and Sayan Mountains. In: Problems of Geocosmos – 2022. Proceedings of the XIV School-Conference with an International Participation (October 3–7, 2022). Skifia-Print, Saint Petersburg, p. 84–92 (in Russian) [Сычева Н.А., Сычев В.Н. Некоторые характеристики сейсмичности Алтая и Саян // Проблемы геокосмоса – 2022: Материалы XIV школы-конференции с международным участием (3–7 октября 2022 г.). СПб.: Скифия-принт, 2022. С. 84–92].

Vakov A.V., 1988. Relationships Between Earthquake Magnitude and Source Dimensions at Different Types of Fault Movements. Collection of Gidroproekt Scientific Papers. Iss. 130. Energoizdat, Moscow, p. 55–69 (in Russian) [Ваков А.В. Соотношения магнитуды и размеров очагов землетрясений при различных типах подвижек // Сборник научных трудов Гидропроекта. М.: Энергоиздат, 1988. Вып. 130. С. 55–69].

Zakharova A.I., Chepkunas L.S., Malyanova L.S., 2009. Source Parameters of Strong Earthquakes. Earthquakes of the Northern Eurasia. Iss. 12 (2003). GS RAS, Obninsk, p. 255–260 (in Russian) [Захарова А.И., Чепкунас Л.С., Малянова Л.С. Очаговые параметры сильных землетрясений Земли // Землетрясения Северной Евразии. Обнинск: ГС РАН, 2009. Вып. 12 (2003 г.). С. 255–260].

Zavyalov A.D., Zotov O.D., 2021. A New Way to Determine the Characteristic Size of the Source Zone. Journal of Volcanology and Seismology 15 (1), 19–25. https://doi.org/10.1134/S0742046321010139.

APPENDIX 1

Table 1.1. Dynamic parameters of earthquakes (69 events) in the Altai-Sayan mountain region

No.	Date	Time	φ, °	λ, °	H, km	M_W	$M_0 \cdot 10^{17}$ (N·m)	r_B, m	$\Delta\sigma$, MPa	$e_{PR} \cdot 10^{-3}$	r_B norm	$\Delta\sigma$ norm
1	03.08.1978	06:07:41.10	52.45	96.96	10.0	5.6	3.60	3020	5.72	0.69	0.19	0.56
2	16.08.1981	17:54:18.10	50.84	97.02	15.0	5.2	0.70	1995	3.86	0.46	0.13	0.37
3	03.08.1982	04:50:29.60	49.01	89.64	10.0	5.1	0.62	1799	4.67	0.56	0.11	0.45
4	24.04.1986	00:22:17.20	47.33	89.54	33.0	5.0	0.43	1622	4.44	0.53	0.10	0.43
5	04.11.1986	16:19:20.20	50.32	88.81	15.0	5.5	2.44	2723	5.29	0.63	0.17	0.51
6	18.09.1987	21:58:39.90	47.24	89.69	15.0	5.3	1.28	2213	5.17	0.62	0.14	0.50
7	30.06.1988	15:25:13.90	50.27	91.13	15.0	5.3	1.01	2213	4.08	0.49	0.14	0.40
8	23.07.1988	07:38:15.00	48.88	91.04	18.0	5.9	8.99	4121	5.62	0.67	0.26	0.55
9	14.06.1990	12:47:32.60	47.88	85.19	36.0	6.6	97.30	8511	6.90	0.83	0.54	0.67
10	03.08.1990	09:15:12.50	48.25	85.28	32.0	6.1	19.80	5070	6.65	0.80	0.32	0.65
11	27.12.1991	09:09:45.80	51.12	98.14	15.0	6.3	37.50	6237	6.76	0.81	0.39	0.66
12	22.06.1995	01:01:23.80	50.30	89.87	15.0	5.4	1.67	2455	4.94	0.59	0.15	0.48
13	29.06.1995	23:02:33.10	51.72	102.71	15.0	5.7	5.20	3350	6.05	0.73	0.21	0.59
14	12.03.1996	18:43:48.30	48.46	88.27	17.0	5.5	2.56	2723	5.55	0.67	0.17	0.54
15	12.07.1998	07:16:21.20	47.79	82.78	35.4	5.2	0.67	1995	3.68	0.44	0.13	0.36
16	21.11.1998	16:59:54.10	49.21	88.89	15.0	5.2	0.74	1995	4.08	0.49	0.13	0.40
17	25.02.1999	18:58:39.00	51.97	104.83	21.0	5.9	8.91	4121	5.57	0.67	0.26	0.54
18	31.05.2000	16:28:07.80	51.47	104.92	15.0	5.0	0.38	1622	3.91	0.47	0.10	0.38
19	07.05.2003	02:58:02.01	48.45	89.57	33.0	5.1	0.64	1799	4.78	0.57	0.11	0.46
20	**27.09.2003**	**11:33:36.25**	**50.02**	**87.86**	**15.0**	**7.2**	**938.00**	**15849**	**10.31**	**1.24**	**1.00**	**1.00**
21	27.09.2003	18:52:52.93	50.09	87.75	15.0	6.4	45.20	6918	5.97	0.72	0.44	0.58
22	01.10.2003	01:03:29.98	50.24	87.59	15.0	6.6	113.00	8511	8.02	0.96	0.54	0.78
23	04.10.2003	14:23:29.00	49.87	88.26	0	3.7	0.00	422	2.61	0.31	0.03	0.25
24	05.10.2003	16:21:13.00	50.16	87.64	0	4.4	0.05	871	3.32	0.40	0.05	0.32
25	06.10.2003	18:30:17.40	50.24	87.65	0	4.2	0.03	708	3.10	0.37	0.04	0.30
26	09.10.2003	16:06:03.16	49.75	88.05	15.0	5.0	0.41	1622	4.24	0.51	0.10	0.41
27	13.10.2003	05:26:42.32	50.25	87.75	15.0	5.1	0.60	1799	4.51	0.54	0.11	0.44
28	17.10.2003	05:30:25.90	50.27	87.94	15.0	5.1	0.61	1799	4.55	0.55	0.11	0.44
29	23.10.2003	00:25:48.46	49.64	88.16	15.0	5.1	0.48	1799	3.64	0.44	0.11	0.35
30	11.11.2003	22:42:35.69	50.47	86.97	15.0	5.1	0.53	1799	3.95	0.47	0.11	0.38
31	17.11.2003	01:35:52.31	50.24	87.53	15.0	5.2	0.75	1995	4.15	0.50	0.13	0.40
32	15.02.2005	12:41:45.28	47.69	89.61	13.2	4.6	0.10	1072	3.70	0.44	0.07	0.36
33	27.04.2005	07:36:15.28	51.09	98.33	12.0	5.3	1.28	2213	5.17	0.62	0.14	0.50
34	22.08.2005	08:31:25.94	49.97	87.63	27.4	4.7	0.13	1189	3.31	0.40	0.07	0.32
35	19.01.2008	07:32:31.71	51.26	98.14	12.0	5.1	0.49	1799	3.69	0.44	0.11	0.36
36	29.01.2008	20:02:30.72	49.74	83.48	34.8	4.9	0.27	1462	3.82	0.46	0.09	0.37
37	16.08.2008	04:01:11.67	52.16	98.31	28.2	5.7	4.70	3350	5.47	0.66	0.21	0.53
38	27.08.2008	01:35:38.61	51.76	104.02	23.5	6.3	34.10	6237	6.15	0.74	0.39	0.60
39	04.08.2009	16:20:43.23	50.66	96.89	30.4	5.3	1.05	2213	4.24	0.51	0.14	0.41
40	10.02.2011	05:35:17.82	52.22	91.76	26.3	5.5	1.89	2723	4.10	0.49	0.17	0.40
41	27.12.2011	15:22:03.84	51.78	95.91	19.5	6.7	138.00	9441	7.18	0.86	0.60	0.70
42	26.02.2012	06:17:24.34	51.69	96.00	20.5	6.6	119.00	8511	8.44	1.01	0.54	0.82
43	26.02.2012	11:59:05.84	51.74	96.03	17.6	5.1	0.54	1799	4.02	0.48	0.11	0.39
44	06.06.2012	14:04:17.47	51.77	96.02	28.0	5.2	0.78	1995	4.31	0.52	0.13	0.42
45	27.07.2012	03:58:13.43	51.73	96.03	17.9	4.9	0.25	1462	3.46	0.41	0.09	0.34

Table 1.1 (continued)

No.	Date	Time	φ, °	λ, °	H, km	M_W	$M_0 \cdot 10^{17}$ (N·m)	r_B, m	$\Delta\sigma$, MPa	$e_{PR} \cdot 10^{-3}$	r_B norm	$\Delta\sigma$ norm
46	30.07.2012	22:30:43.73	50.61	87.36	25.9	5.1	0.57	1799	4.29	0.51	0.11	0.42
47	24.01.2013	07:35:37.30	49.80	87.75	19.6	5.2	0.76	1995	4.16	0.50	0.13	0.40
48	30.04.2013	01:03:33.34	51.35	92.64	12.0	5.0	0.39	1622	3.98	0.48	0.10	0.39
49	01.11.2014	00:52:01.56	52.70	101.45	29.8	4.8	0.19	1318	3.59	0.43	0.08	0.35
50	05.12.2014	18:04:22.68	51.33	100.72	22.8	5.0	0.35	1622	3.61	0.43	0.10	0.35
51	13.07.2016	06:45:48.63	49.93	89.77	31.2	4.9	0.28	1462	3.93	0.47	0.09	0.38
52	20.09.2016	07:18:14.06	49.90	88.06	18.7	4.8	0.23	1318	4.35	0.52	0.08	0.42
53	04.04.2017	15:07:31.43	47.28	85.08	32.6	5.3	0.96	2213	3.89	0.47	0.14	0.38
54	01.02.2019	21:54:43.19	46.78	83.39	26.0	5.0	0.46	1622	4.67	0.56	0.10	0.45
55	29.03.2019	23:22:06.97	51.65	101.57	21.9	4.8	0.20	1318	3.90	0.47	0.08	0.38
56	13.09.2019	04:08:04.81	50.57	87.45	20.7	5.1	0.63	1799	4.70	0.56	0.11	0.46
57	21.09.2020	18:05:00.13	51.85	103.50	25.9	5.5	2.49	2723	5.40	0.65	0.17	0.52
58	21.09.2020	18:19:58.18	51.80	103.48	18.5	4.8	0.20	1318	3.74	0.45	0.08	0.36
59	11.01.2021	21:33:07.45	51.32	100.39	13.9	6.8	190.00	10471	7.24	0.87	0.66	0.70
60	13.01.2021	11:10:11.81	51.63	100.61	12.0	4.8	0.18	1318	3.48	0.42	0.08	0.34
61	21.02.2021	01:37:08.94	52.33	97.44	27.4	5.0	0.36	1622	3.73	0.45	0.10	0.36
62	31.03.2021	00:01:29.29	51.24	100.45	24.9	5.3	1.02	2213	4.12	0.49	0.14	0.40
63	03.05.2021	08:46:41.95	51.31	100.43	27.5	5.7	4.21	3350	4.90	0.59	0.21	0.48
64	06.09.2021	07:47:21.91	53.20	99.23	24.9	5.3	1.05	2213	4.24	0.51	0.14	0.41
65	22.10.2021	23:03:04.95	51.39	91.67	29.8	5.0	0.42	1622	4.28	0.51	0.10	0.42
66	29.07.2022	13:01:14.18	50.40	90.70	13.0	5.5	2.37	2723	5.14	0.62	0.17	0.50
67	14.01.2023	07:39:34.60	51.08	100.03	19.9	4.9	0.26	1462	3.67	0.44	0.09	0.36
68	04.03.2023	01:18:25.17	51.04	98.28	19.7	4.8	0.17	1318	3.27	0.39	0.08	0.32
69	15.02.2025	01:48:13.11	50.03	88.24	26.0	5.8	6.20	3715	5.29	0.63	0.23	0.51